

Carbon Storage | Hot Paper |

Effect of Building Block Transformation in Covalent Triazine-Based Frameworks for Enhanced CO₂ Uptake and Metal-Free Heterogeneous Catalysis

Himanshu Sekhar Jena^{+, * [a]}, Chidharth Krishnaraj^{+, [a]}, Johannes Schmidt,^[b] Karen Leus,^[a] Kristof Van Hecke,^[c] and Pascal Van Der Voort^{* [a]}

Abstract: Covalent triazine frameworks (CTFs) have provided a unique platform in functional material design for a wide range of applications. This work reports a series of new CTFs with two new heteroaromatic building blocks (pyrazole and isoxazole groups) through a building-block transformation approach aiming for carbon capture and storage (CCS) and metal-free catalysis. The CTFs were synthesized from their respective building blocks [(4,4'-(1*H*-pyrazole-3,5-diyl)dibenzonitrile (pyz) and 4,4'-(isoxazole-3,5-diyl)dibenzonitrile (isox))] under ionothermal conditions using ZnCl₂. Both of the building blocks were designed by an organic transformation of an acetylacetone containing dinitrile linker to pyrazole and isoxazole groups, respectively. Due to this organic transformation, (i) linker aromatization, (ii) higher surface areas and nitrogen contents, (iii) higher aromaticity, and (iv) higher sur-

face basicity was achieved. Due to these enhanced properties, CTFs were explored for CO₂ uptake and metal-free heterogeneous catalysis. Among all, the isox-CTF, synthesized at 400 °C, showed the highest CO₂ uptake (4.92 mmol g⁻¹ at 273 K and 2.98 mmol g⁻¹ at 298 K at 1 bar). Remarkably, these CTFs showed excellent metal-free catalytic activity for the aerobic oxidation of benzylamine at mild reaction conditions. On studying the properties of the CTFs, it was observed that organic transformations and ligand aromatization of the materials are crucial factors to tune the important parameters that influence the CO₂ uptake and the catalytic activity. Overall, this work highlights the substantial effect of designing new CTF materials by building-block organic transformations resulting in better properties for CCS applications and heterogeneous catalysis.

Introduction

Over the past few years, tremendous efforts have been devoted to the development of porous organic polymers (POPs).^[1] This sort of polymeric material is a potential candidate for carbon capture storage (CCS)^[2] and carbon capture utilization (CCU)^[1] applications. CCS and CCU are considered as potential technologies that can tackle the current biggest scientific challenges and have a positive impact on the environment as well as the economy. In the view of the growing population and

fulfilling energy demands, it is also necessary to develop more efficient, greener and more sustainable chemical industries by designing renewable solid catalysts.^[3] Considering these two important applications, POPs are considered as smart materials for their unique characteristics (large surface area, tunable pore volume, functionalities and high stability).


Among all, covalent triazine frameworks (CTFs)^[4] have proven to be a highly promising class of materials because of their easy synthesis, high stability, and most importantly low-density network. In addition, they are highly reproducible and can be reused multiple times in a cost-effective way. Therefore, significant attention has been given for engineering CTFs with different heteroaromatic functional groups for CCS and heterogeneous catalysis.^[4a-c] Particularly, to achieve enhanced CO₂ uptake, CTFs are engineered with different CO₂-philic aromatics like pyridine, bipyridine,^[5] benzimidazole,^[6] fluorene,^[7] carbazole,^[8] porphyrin, perfluorinated,^[9] and triazole^[10] backbones to enhance the Lewis acid–base interactions. Incorporation of heteroatoms (N, O, S) is another potential route to achieve enhanced CO₂ uptake because of higher dipole–quadrupole interactions.^[11] CTFs also showed promising applications in supported metal ion or nanoparticle-based heterogeneous catalysis.^[12] Additionally, CTFs have also been used as metal-free catalysts for the cycloaddition of CO₂ to various epoxides,^[13] oxidative cleavage of lignin model compounds^[14] and also as

[a] Dr. H. S. Jena,⁺ C. Krishnaraj,⁺ Dr. K. Leus, Prof. Dr. P. Van Der Voort
Center for Ordered Materials, Organometallics and Catalysis (COMOC)
Department of Chemistry, Ghent University
Krijgslaan 281 (S3 B), 9000 Ghent (Belgium)
E-mail: himanshu.jena@ugent.be
Pascal.VanDerVoort@UGent.be

[b] Dr. J. Schmidt
Technische Universität Berlin, Institut für Chemie—Funktionsmaterialien
Hardenbergstraße 40, 10623 Berlin (Germany)

[c] Prof. Dr. K. Van Hecke
XStruct, Department of Chemistry, Ghent University
Krijgslaan 281 (S3 B), 9000 Ghent (Belgium)

[*] These authors contributed equally to this work.

 Supporting information and the ORCID identification number(s) for the author(s) of this article can be found under:
<https://doi.org/10.1002/chem.201903926>

organocatalysts^[15] in carbene-catalyzed conjugated umpolung reactions. So far, the excellent catalytic properties of CTF are claimed to be due to the presence of different types of nitrogen (pyridinic, pyrrolic, quaternary and pyridinic N-oxide) even though it is still unclear which specific type of nitrogen is responsible in a particular reaction. Recently, chemical activation of CTF by KNO₃ and KOH were used to obtain enhanced CO₂ uptake^[16] and high reactivity, respectively, in the oxidation of methylene compounds.^[17] It was shown that KOH and KNO₃ activation enhanced the basicity of CTF materials, resulting in improved properties. Recently, Giambastiani et al. reported that the gas adsorption capacity and organocatalytic activity of CTFs can be modulated through an appropriate selection of the building blocks.^[18] Their results showed that neither purely microporous samples (highly N-rich) nor mesoporous and N-poor CTFs were ideal candidates for the CO₂ capture and storage. However, the correct combination of surface area, N content and micro-mesoporous morphology of CTFs are necessary to obtain the highest CO₂ uptake.

Herein, we highlight the effect of organic transformations and ligand aromatization to tune the surface area, N content, pore characteristics, and surface basicity of CTFs to achieve enhanced CO₂ uptake and metal-free catalytic activity.

Experimental Section

The required chemicals were purchased from Sigma-Aldrich and used without further purifications. The ¹H and ¹³C NMR analysis of the dinitrile linker were measured using a 300 MHz spectrometer. Elemental analyses (C, H, N, and O) were carried out on a Thermo Scientific Flash 2000 CHNS-O analyzer equipped with a TCD detector. Fourier Transform Infrared Spectroscopy (FT-IR) in the region of 4000–650 cm⁻¹ was performed with a Thermo Nicolet 6700 FT-IR spectrometer equipped with a nitrogen-cooled MCT detector and a KBr beam splitter. Dinitrogen (N₂) adsorption isotherms were obtained using a Belsorp Mini apparatus measured at 77 K, whereas CO₂ and H₂ adsorption measurements were carried out on a Quantachrome iSorb-HP gas sorption analyzer at respective temperatures and 1 bar pressure. TPD-CO₂ measurements were performed in a Quantachrome Autosorb-iQ TPX with a flow of CO₂/He (5/95) mixture. Powder X-ray diffraction (PXRD) patterns were collected on a Thermo Scientific ARL X'Tra diffractometer, operated at 40 kV, 30 mA using Cu-Kα radiation (λ = 1.5406 Å). Thermogravimetric analysis (TGA) were performed on a Netzsch STA-449 F3 Jupiter-simultaneous TG-DSC analyzer in a temperature range of 20–800 °C under N₂ atmosphere and a heating rate of 2 °C min⁻¹. The degree of carbonization was calculated using equation from ref. [26]. Pore size distributions were determined using the calculation model for Ar at 87 K on carbon (slit pore, QSDFT equilibrium model) of the ASiQwin software (v1.27) from Quantachrome. The X-ray photoelectron spectroscopy (XPS) measurements were performed on a Thermo Fisher Scientific K-Alpha 250 Xi. For the structure of the 4,4'-(1H-pyrazole-3,5-diyl)dibenzonitrile (pyz), X-ray intensity data were collected on an Agilent Supernova Dual Source (Cu at zero) diffractometer equipped with an Atlas CCD detector using CuKα radiation (λ = 1.54178 Å) and ω scans. The images were interpreted and integrated with the program CrysAlisPro (Agilent Technologies).^[19] Using Olex2,^[20] the structure was solved by direct methods using the ShelXS structure solution program and refined by full-matrix least-squares on F² using the ShelXL program package.^[21]

Non-hydrogen atoms were anisotropically refined and the hydrogen atoms in the riding mode and isotropic temperature factors fixed at 1.2 times U(eq) of the parent atoms.

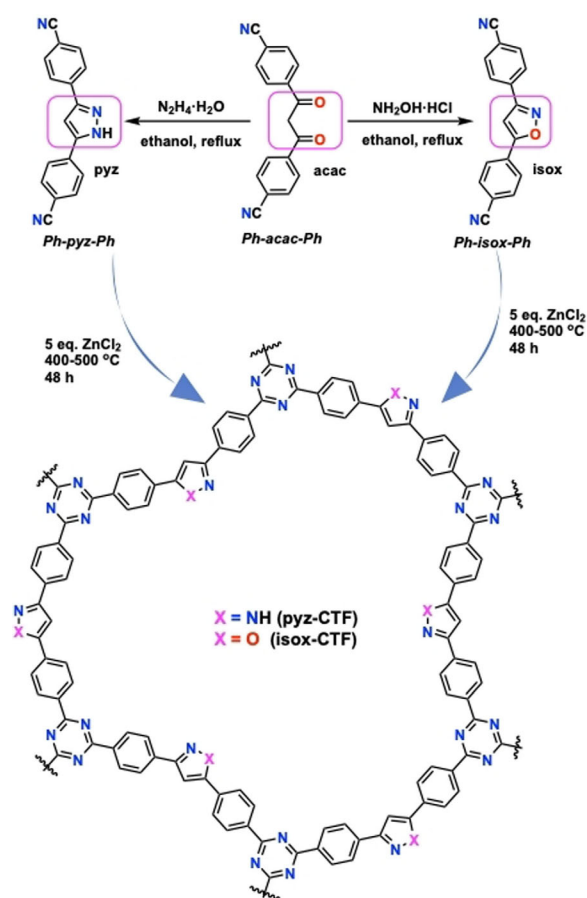
Supporting Information

This file contains detailed experimental procedure with Table, Scheme, NMR and LC-MS data of both ligands, elemental analysis, XPS analysis, powder X-ray diffraction analysis, thermogravimetric analysis, single crystal X-ray structure of 4,4'-(1H-pyrazole-3,5-diyl)dibenzonitrile, CO₂/N₂ selectivity using Henry and IAST methods, Q_{ST} plots of all CTF materials, recyclability test and X-ray diffraction results of 4,4'-(1H-pyrazole-3,5-diyl)dibenzonitrile; the crystallographic data is also accessible. CCDC 1914227 contains the supplementary crystallographic data for this paper. These data are provided free of charge by The Cambridge Crystallographic Data Centre.

Results and Discussion

Synthesis and characterization of CTFs

So far, four synthetic methods have been used for CTF synthesis; ionothermal synthesis,^[5c] room temperature and microwave synthesis using CF₃SO₃H,^[22] polycondensation of aldehydes and amidines at 120 °C^[23] and direct synthesis using P₂O₅-catalyzed condensation of aromatic amides.^[24] However, most of the CTFs are synthesized using the ionothermal method as it is



Scheme 1. Scheme illustrating linker synthesis and their respective covalent triazine frameworks synthesized under ionothermal conditions.

less stringent on linkers and is highly reproducible. Using this method, herein two sets of CTFs were synthesized from their respective dinitrile linkers (4,4'-(1*H*-pyrazole-3,5-diyl)dibenzonitrile (pyz) and 4,4'-(isoxazole-3,5-diyl)dibenzonitrile (isox) (Scheme 1). Details about the synthesis and characterization of both the dinitrile linkers/building units are described in the Supporting Information (Figures S1–S6). Further on, they are referred to as pyz-CTF-*x-y* and isox-CTF-*x-y*, where, *x*=ZnCl₂ equivalents and *y*=synthesis temperature (Table S1). Notably, these two linkers (pyz and isox) were easily obtained from 4,4'-malonyldibenzonitrile (acac) upon simple condensation reactions, with hydrazine hydrate and hydroxylamine hydrochloride, respectively. As shown in Scheme 1, the organic transformation resulted in extended fused aromatic rings (phenyl-pyrazole-phenyl and phenyl-isoxazole-phenyl) with polar functional sites (N[∧]N and N[∧]O) from a flexible phenyl-acac-phenyl containing dinitrile linker. The new sets of CTF materials are characterized well and explored for gas adsorption, separation, and metal-free heterogeneous catalysis. The results were compared

with acac-CTF^[11f] and CTF-1^[5b,c] and other CTFs were included wherever necessary.

Characterization of CTFs

For the preliminary characterization, FT-IR measurements were undertaken to confirm the complete trimerization of the nitrile group to a triazine ring (Figure 1a). Notably, the absence of a –CN band at 2229 cm⁻¹ and presence of a –C=N (triazine) band at 1598 cm⁻¹ confirmed the complete conversion of the nitrile groups to triazine rings ensuring the CTF formation. In all the CTFs, the two sharp peaks observed at around 2850 and 2900 cm⁻¹ are the C–H stretching bands of the –CH₂ group of five-membered ring due to partial decomposition of ligands at elevated temperatures.^[9b,11f,g,25]

From the elemental analysis (Table 1 and Table S2), the observed increase in N content from acac-CTF^[11f] to pyz-CTF and isox-CTF confirmed the formation of both CTFs with the respective functional groups. However, the obtained results indi-

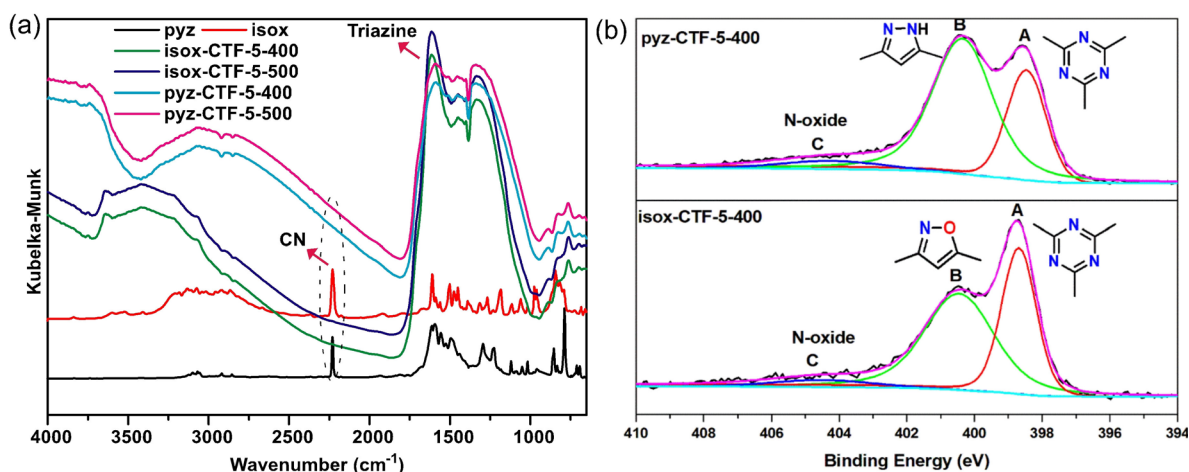


Figure 1. (a) FT-IR spectral comparison between linkers and respective CTFs and (b) deconvoluted XPS N 1s spectra of pyz-CTF-5-400 and isox-CTF-5-400.

Entry	CTF	S _A ^{BET} ^[a] (m ² g ⁻¹)	V _t ^[b] (cm ³ g ⁻¹)	N (%) ^[c]	C/N	CO ₂ uptake (mmol g ⁻¹) 273 K 298 K	Q _{st} ^[d] (kJ mol ⁻¹)	CO ₂ /N ₂ ^[e]	H ₂ (wt %)	Ref.
1	pyz-CTF-5-400	1605	0.81	10.888	7.23	3.82 2.19	27	26 (72)	1.78	this work
2	pyz-CTF-5-500	1405	0.85	8.914	7.96	3.31 1.96	27	18 (84)	1.31	this work
3	isox-CTF-5-400	1683	0.70	7.467	7.18	4.92 2.86	29	29 (83)	1.60	this work
4	isox-CTF-5-500	1537	0.72	7.917	8.99	4.23 2.69	25	18 (88)	1.32	this work
5	acac-CTF-5-500	1556	1.20	5.070	16.27	3.30 1.97	28	46	1.53	[11f]
6	CTF-1-400	610	0.98	18.60	3.77	2.83 1.52	33.7	59	–	[5a]
7	bipy-CTF-600	2479	1.24	13.61	4.96	5.58 2.95	34.4	37	2.10	[5a]
8	F-DCBP-CTF-400	1574	1.50	11.3	5.28	5.98 3.82	33.1	31	1.77	[9b]
9	HAT-CTF-450/600	1090	0.263 ^[f]	32.8 ^[g]	–	6.3 4.80	27.1	126	–	[11b]
10	df-TzCTF-600	1720	1.12	8.26	7.05	6.9 4.60	34	21	2.50	[10a]
11	Tz-df-CTF-600	2106	1.43	6.15	7.86	7.65 5.08	20.0	21.1	2.91	[10b]

[a] BET surface area was calculated over the relative pressure range of 0.01–0.05 at 77 K. [b] V_t, total pore volume was calculated at P/P₀=0.98. [c] Percentage of nitrogen content calculated from elemental analysis. [d] Calculated isosteric heat of adsorption of CO₂ using the Clausius–Clapeyron equation. [e] The selectivity of material for CO₂ adsorption over N₂ at 298 K was calculated by taking initial slopes in the Henry region of the respective gases, whereas values in parenthesis were calculated by ideal adsorbed solution theory (IAST) method at a molar ratio of 15:85 for CO₂/N₂. [f] estimated from CO₂ isotherm. [g] XPS analysis.

cate a lower number of heteroatoms and a higher C content than the expected value. To obtain a more detailed picture, the degree of carbonization was calculated. 9–12% carbonization was found in the CTFs.^[26] As can be seen from Table 1, the C/N ratio slightly increases with increase in the synthesis temperature, which is comparable to the reported CTF materials.

Further, the nature of elements corresponding to the functional groups and their binding energy were characterized by XPS measurements. XPS spectra of pyz-CTF-5-400 and isox-CTF-5-400 were measured and analyzed by fitting the respective atoms to their binding energies.^[27] For pyz-CTF-5-400, in the obtained XPS spectra, C 1s (deconvoluted) peaks at 284 eV and 285 eV can be assigned to C–C/C–H and C–N species, respectively (Figure S7). The N 1s spectrum of pyz-CTF-5-400 showed two peaks at 398 eV (A) and 400 eV (B), which can be assigned to the phenyl functionalized triazine (A) and pyrrolic-NH species (B), respectively (Figure 1). For isox-CTF-5-400, the C 1s spectra are very similar to pyz-CTF-5-400 (Figure S7); however, in the N 1s spectra, a significant decrease in intensity of the peak at 400 eV with respect to 398 eV was noticed. This is due to the absence of pyrrolic-NH function in the isoxazole unit, which was replaced by an oxygen atom and hence the decrease in the peak intensity was observed. Even in the absence of pyrrolic N-species for isox-CTF, a peak at ≈ 400 eV appears. It is common to observe pyrrolic NH for almost all CTF materials under ionothermal conditions rearrangements regardless of the nature of their functional groups. However, the decrease in intensity clearly confirmed the transformation of pyrazole to isoxazole and retention of respective groups even after ionothermal synthesis.

To explore the phase purity and nature of the CTF materials, powder X-ray diffraction (PXRD) measurements were undertaken (Figure S8). Based on the results, all the CTFs showed a very broad peak in the range of $2\theta = 20\text{--}24^\circ$ corresponding to the two-dimensional layers stacked on each other by $\pi\cdots\pi$ interactions.^[5c] The stability of all the CTFs was verified by TGA analysis under N_2 atmosphere, which showed that they are robust like other reported CTFs and are stable up to 500°C (Figure S9).

Gas sorption properties

After these preliminary characterizations, CTF materials were activated under vacuum at 150°C overnight. The surface area properties of all these activated CTF materials were determined from N_2 sorption measurements at 77 K (Figure 2). The respective surface areas and total pore volumes (V_t) calculated at $P/P_0 = 0.98$ are displayed in Table 1. As shown in Figure 2, the obtained isotherms for all these CTF materials resemble type-I adsorption isotherm. As summarized in Table 1, the BET surface area (SA_{BET}) of both set of CTFs decreases upon increase in temperature. However, in both sets of materials, the total pore volume (V_{tot}) increases with respect to temperature (entries 1–4; Table 1). Notably, the observed SA_{BET} and V_t of pyz-CTFs and isox-CTFs differ significantly from acac-CTF (entry 5). From XPS, PXRD, TGA, and N_2 sorption analysis, it was confirmed that both sets of CTF materials are robust with large surface area

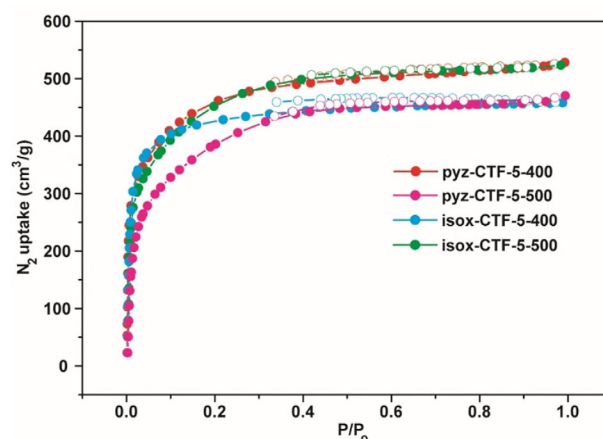


Figure 2. Nitrogen adsorption/desorption isotherms of pyz-CTFs and isox-CTFs measured at 77 K, filled and empty symbols represent adsorption and desorption, respectively.

and different kind of N-sites (due to triazine and pyrazole/isoxazole groups) uniformly distributed over the materials. In general, these kinds of N-sites interact strongly with CO_2 due to dipolar interactions. Therefore, these materials were used to evaluate their CO_2 adsorption and selectivity over N_2 .

CO_2 adsorption/desorption isotherms were recorded at 273 K and 298 K at 1 bar of pressure (Figure 3). The uptake of both sets of CTF materials at respective temperatures are included in Table 1.

The best CO_2 uptake was obtained for isox-CTF-5-400 with values of 4.92 mmol g^{-1} at 273 K and 2.86 mmol g^{-1} at 298 K and 1 bar, respectively (entry 3; Table 1). In general, for previously reported CTFs, larger surface area, greater number of heteroatoms, and a high degree of microporosity collectively resulted in high CO_2 uptake. When comparing the two sets of CTF materials (entries 1–4), it was found that isox-CTF-5-400

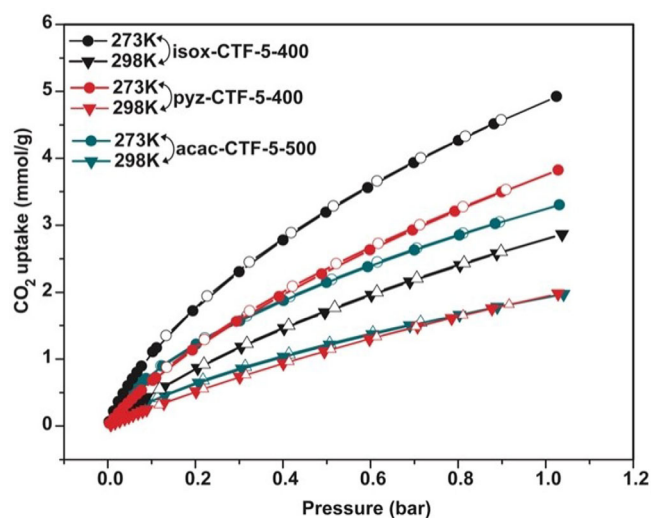


Figure 3. CO_2 adsorption/desorption isotherms of pyz-CTF-5-400 and isox-CTF-5-400 measured at 1 bar, filled and empty symbols represent adsorption and desorption, respectively.

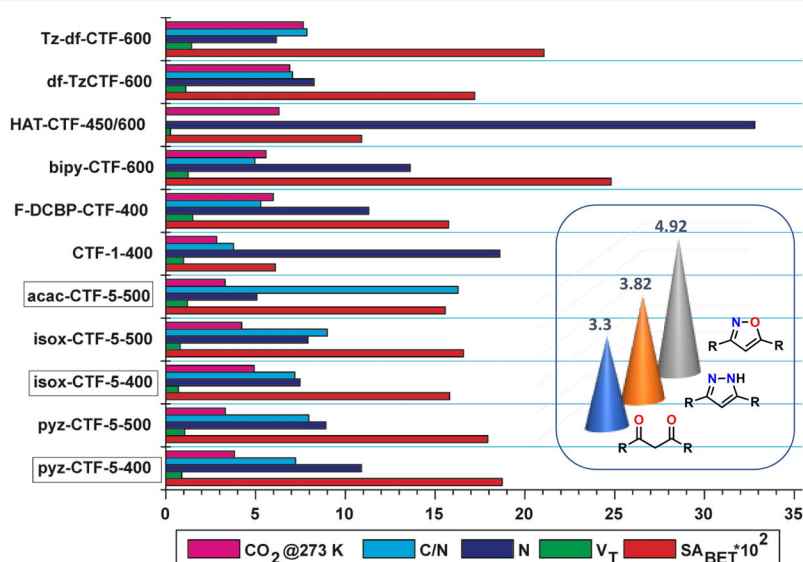


Figure 4. CO₂ uptake of CTF materials versus their BET surface area, total pore volume, nitrogen content and C/N ratio measured at 273 K and 1 bar (inset shows a comparison of CO₂ uptake in mmol g⁻¹ of acac-CTF, pyz-CTF and isox-CTF at 1 bar of pressure). Note: CO₂ uptake in mmol g⁻¹, C/N ratio is wt%/wt%, N in wt%, V_T in cm³ g⁻¹ and SA_{BET} in m² g⁻¹.

with highest surface area and lowest total pore volume (0.70 cm³ g⁻¹) showed the best CO₂ uptake.

In order to compare the observed CO₂ uptake properties with reported values, a few representative CTFs with different surface area, pore volume, nitrogen content and C/N ratio were included in Table 1 (entries 5–11). On comparison, it can be stated that CO₂ capacities of the present new sets of CTF materials are higher than acac-CTFs, DCI-CTF, CTF-1, and are comparable with many other CTFs with different heteroaromatic groups.^[5a, 6, 7, 9d, 11f, 18, 25, 26] However, they are lower than that observed in bipy-CTF-600 (5.58 mmol g⁻¹),^[5a] F-DCBP-CTF^[9b] (5.98 mmol g⁻¹), HAT-CTF-450/600^[11b] (6.3 mmol g⁻¹), and triazole containing CTFs^[10] (7.65 mmol g⁻¹) (entries 7–12). In order to gain more insight, the CO₂ uptake of each CTF was plotted with respect to its surface area, pore volume, nitrogen content, and C/N ratio; respective values are plotted into a bar graph (Figure 4). From this it can be concluded that all the three parameters (surface area, pore volume, and nitrogen content) have significant role in CCS application.^[2c, 18, 28] In order to further investigate the difference in CO₂ capacities of isox-CTF and pyz-CTFs, the isosteric heats of adsorptions (Q_{st}) of CO₂ were calculated using the Clausius–Clapeyron equation (Figure S10). From the obtained values in Table 1, it was found that isox-CTF-5-400 showed the highest Q_{st} value (29 kJ mol⁻¹), confirming that the former exhibited the strongest interaction with CO₂ among these four CTFs and corroborated with the highest CO₂ value. Notably, the calculated Q_{st} values are higher than the heat of liquefaction of CO₂ (17 kJ mol⁻¹)^[29] and are comparable to most of the reported CTFs at similar conditions.^[4a, c]

In addition to the CO₂ storage, CTFs are promising materials for CO₂ separation from a mixture of gases. In particular, they showed promising application in CO₂/N₂ separation because of their robustness, large surface areas, and high N content

(Table 1). Therefore, to explore the potential of pyz-CTF and isox-CTF materials in CO₂/N₂ separation, the selectivity was calculated using the Henry law by using the ratio of the slopes of the CO₂ adsorption isotherms (<0.06 bar) and N₂ (<0.1 bar) at 298 K (Figures S11 and S12). The obtained values in Table 1, represent the moderate CO₂/N₂ selectivity of these materials. The best value was 29 for isox-CTF-5-400. In addition, the selectivity was calculated using ideal adsorbed solution theory (IAST) method at 298 K using binary mixture of CO₂ and N₂ gas (CO₂/N₂ = 15/85).^[5a, 10] In this study, experimental adsorption isotherms data for CO₂ and N₂ at 298 K were fitted to the single-site Langmuir model for CO₂ and N₂ isotherms, purely on the basis of giving the best fit with highest R₂ values (Figure S13 and Table S3). The selectivity values are listed in Table 1. The value listed in Table 1 show a large difference between Henry and IAST methods. Higher selectivity values towards CO₂ were obtained by IAST model at low pressure range, which decreases with increase in working pressures (Figure S14). The isox-CTFs showed higher selectivity values than pyz-CTFs. The obtained values are comparable with most of the CTFs^[4c] but less than HAT-CTF-450/600^[11b] (126; entry 9; Table 1) and pym-CTF-500 (503).^[5a] Furthermore, in order to obtain a deeper insight in the observed CO₂ adsorption and CO₂/N₂ selectivity with respect to the pore of the CTF materials, pore size distributions of three best CTFs (isox-CTF-5-400, pyz-CTF-5-400 and acac-CTF-5-500) were performed based on Ar-sorption using QSDFT calculations. As shown in Figure S15, two peaks of pore sizes around 0.9 and 1.7 nm were observed in three CTFs. However, in acac-CTF-5-500 an additional peak around 2.7 nm was observed which is due to increase in amount of supermicropores or small mesopores.^[5a] This observation is well corroborated with the type IV BET isotherm of it reported earlier.^[11f] Therefore, in this case, it is difficult to correlate the observed difference in CO₂ uptake with their pore

sizes. From the above discussed CO₂ uptake studies, it can be concluded that modification of building units (conversion of acetylacetone to pyrazole and isoxazole) with increase heteroatoms resulted in a significant enhancement of CO₂ uptake (Figure 3). It can be attributed to the strong dipolar interactions between different N elements (triazine-N, pyridinic-N, pyrrolic-N and oxidized N–O species) obtained under the ionothermal condition and the internal pyrazole and isoxazole groups with CO₂ molecules. In addition, different Lewis acid–base interactions between carbon atoms of CO₂ molecule (Lewis acid) and the lone-pair electron on the nitrogen atom (Lewis base) of respective functional groups also play a significant role in high CO₂ adsorption.^[5] Although these new CTFs do not achieve the best amount of CO₂ storage, this work emphasizes the impact of a simple transformation of functional groups on the carbon capture properties. Further, to prove the structural properties (surface area and number of heteroatoms) and its correlation with the enhanced CO₂ uptake, single-crystal X-ray analysis of (4,4'-(1*H*-pyrazole-3,5-diyl)dibenzonitrile was performed (Figure S16).^[19–21] As expected, the dihedral angle between two appended benzonitrile groups is increased from 135° (acac) to 151°(pyz/isox). As shown in Scheme S1 (Supporting Information), this difference in dihedral angle resulted in a completely different ideal structure with high surface area and increase in number of hetero atoms. Therefore, the obtained higher CO₂ uptake can be corroborated with both parameters.

Apart from the surface properties, basicity of porous materials is considered an important parameter to achieve higher CO₂ uptake.^[17,30] In general, the basicity of metal-free carbon-based materials is linked to the nature of the nitrogen-based dopant. Particularly in CTFs, four different N-sites/N-dopants for example, pyridinic-N, pyrrolic-N, quaternary-N and N-oxides are uniformly distributed over the surface. Therefore, the overall basicity of CTF materials is linked to these four different N-sites, including chemically accessible or unreachable basic N-sites.^[30]

In particular, surface basicity is an open matter of debate and has a significant influence on CCS and base-catalyzed heterogeneous catalysis.^[3b,c,11e,30] In order to further corroborate the observed CO₂ uptake with surface basicity, temperature-programmed desorption (TPD) of CO₂ analysis of isox-CTF, pyz-CTF, acac-CTF and CTF-1 were performed. As shown in Figure 5, mainly two desorption peaks of CO₂ in the temperature range of 68–160 °C and 190–350 °C were observed (Table 2). These two-desorption peaks signify weak and moderate basic sites, respectively. This observance is quite consistent with similar sorts of reported materials.^[31] The total basicity refers to the total amount of CO₂ desorbed from the materials and therefore it is calculated by taking the weight as well as the surface area of the respective materials into consideration (Table 2).

From the TPD-CO₂ analysis, it is revealed that the basicity of the CTF materials changed with synthesis temperature and nature of building blocks. As represented in Table 2, CTF-1 showed the highest degree of basicity. Among the new sets of CTF materials, isox-CTF-5-400 showed a higher degree of basic-

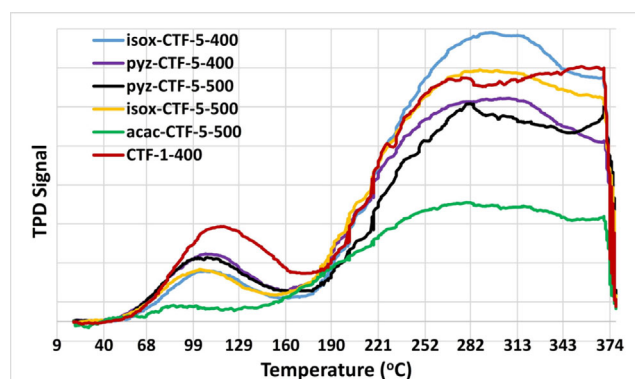


Figure 5. CO₂-TPD of pyz-CTF, isox-CTF, acac-CTF and CTF-1.

CTF	Basicity (mmol g ⁻¹)			CO ₂ ^[b]
	weak	moderate	total ^[a]	
pyz-CTF-5-400	1.021	28.837	29.85(0.016)	3.82
pyz-CTF-5-500	1.289	26.988	28.27(0.015)	3.31
isox-CTF-5-400	1.141	30.560	31.70(0.020)	4.92
isox-CTF-5-500	1.926	24.442	26.36(0.016)	4.23
acac-CTF-5-500	0.076	14.637	14.71(0.009)	3.30
CTF-1-400	3.973	31.912	35.88(0.059)	2.83

[a] Values in the parentheses represent the basicity of respective materials with respect to their surface area (mmol m⁻²). [b] uptake in mmol g⁻¹ at 273 K and 1 bar.

ity than the other pyz-CTFs, isox-CTF, and acac-CTFs. This result clearly substantiates that CTF materials with higher basicity can show high CO₂ uptake. From this study, it can be concluded that simple organic transformation of acetyl acetone to pyrazole and isoxazole groups also influenced the basicity of respective CTFs to a greater extent. Overall, the surface basicity including surface area, pore volume, and number of heteroatoms of any CTF materials have a significant influence on their CO₂ uptake capacities.

Motivated by the enhanced CO₂ uptake and moderate CO₂/N₂ selectivity, H₂ storage properties of these CTF materials were also explored. Recently, CTF materials showed potential to store large amounts of H₂ (bipy-CTF-600; 2.10 wt%, df-TzCTF-600; 2.50 wt%, Tz-df-CTF-600; 2.91 wt%) at 77 K and 1 bar (entries 7, 10, and 11; Table 1).^[5a,10a,b] In order to explore the hydrogen storage properties, the hydrogen adsorption measurements of pyz-CTF and isox-CTF were performed at 77 K (Figure 6) and a hydrogen storage amount of 1.31–1.78 wt% at 1 bar was obtained (entries 1–4; Table 1). Notably, at low hydrogen pressure (0.12 bar), isox-CTF-5-400 showed the highest storage amount (0.9 wt%) but the isotherm was saturated at 0.7 bar of pressure with 1.6 wt% of hydrogen storage (Figure 6, insert). However, in pyz-CTF-5-400, the isotherm was not saturated even at 1 bar and hence exhibited the highest hydrogen storage capacity (1.78 wt%). As noted in Table 1, pyz-CTF-5-400 exhibited slightly higher pore volume and 3.4 wt% higher N content than isox-CTF-5-400. Both of these

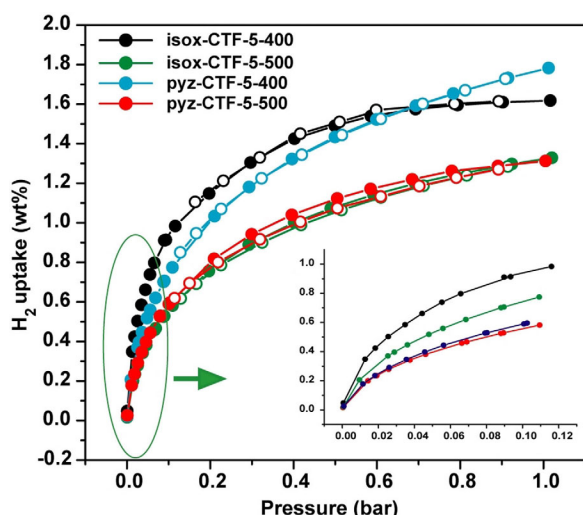


Figure 6. Hydrogen adsorption isotherms of pyz-CTF and isox-CTF at 77 K and 1 bar.

parameters might be responsible for the higher amount of H₂ storage. Additionally, the obtained values are comparable with most of the CTFs obtained from building blocks with pyridine, bipyridine, benzimidazole, carbazole and other functional groups.^[4c,d]

Catalytic properties

The enhanced properties, presence of different N-sites, and surface basicity of these new CTFs prompted us to explore their catalytic activity as solid heterogeneous metal-free catalysts. Recently, development of porous solid bases from simple and efficient methods are attracting interest in green chemistry and heterogeneous catalysis. In general, traditional inorganic bases suffered from many important disadvantages, despite their low cost and easy availability, that is, they often deteriorate the catalytic activity, worsen the separation process and produce waste.^[17] Recently, CTFs have shown significant promise as porous solid base and have been used in base free Ru-catalyzed aqueous phase oxidation^[12h] and Ir-catalyzed transfer hydrogenation,^[12a] and metal-free cycloaddition reaction of CO₂ and epoxides,^[13a] oxidation of methylene compounds,^[17] alcohol oxidations,^[12b] and oxidative cleavage of lignin model compounds.^[14]

Herein, we explored these new CTFs as metal-free heterogeneous catalysts for the aerobic oxidative dimerization of benzyl amine to *N*-benzyl-1-phenylmethanimine as proof-of-concept catalysis. Selective oxidative dimerization of amine to imine, is regarded as an important electrophilic intermediate in organic synthesis.^[32] Although it can be achieved by stoichiometric number of organic bases, effort has been devoted to developing catalysts using simple oxygen/air as terminal oxidant. Different sets of metal-based or metal-free catalysts and photo catalysts have shown good activity for the reaction (Table 3, entry 10–17).^[32,33] However, the key challenge is to avoid formation of two key side products, aldehyde and nitriles, due to the hydrolysis of imine and dehydrogenation of amine, respec-

Table 3. Catalytic test using CTF in the aerobic oxidative dimerization of benzylamine to *N*-benzyl-1-phenylmethanimine.^[a]

Entry	Catalyst	Conversion of 1a [%] ^[b]	Selectivity of 2a [%] ^[b]
1	pyz-CTF-5-400	100	92
2	pyz-CTF-5-500	100	86
3	isox-CTF-5-400	100	98
4	isox-CTF-5-500	100	90
5	acac-CTF-5-500	38	35
6	CTF-1-400	100	> 99
7 ^[c,d,e]	CTF-1-400	100	91
8 ^[f]	graphite oxide ^[33a]	99	98
9 ^[g]	silica templated mesoporous carbon ^[33b]	100	94.2
10 ^[h]	N-doped carbon ^[33c]	98	98
11 ^[i]	mpg-C3N4 ^[32]	99	99
12 ^[j]	WS2 nanosheets ^[33e]	92	95
13 ^[k]	CF-HCP based POPs ^[33f]	100	91
14 ^[f]	MOF-253 ^[33d]	> 99	> 99
15 ^[l]	CTF-p ^[33g]	94	91
16 ^[m]	CTF-1-400	100	> 99
17 ^[n]	CTF-1-400	< 1	-

[a] Reaction conditions: **1a** (2 mmol), CTF catalyst (10 mg), 1 atm of O₂, 24 h, 40 °C and CH₃CN as solvent. [b] Determined from ¹H NMR analysis using mesitylene as internal standard. [c] Air. [d] Solvent free. [e] At room temperature. [f] 100 °C, 5 atm of O₂. [g] 100 °C. [h] 110 °C. [i] 60 °C, 5 atm of O₂ and λ > 420 nm. [j] 80 °C, 60 W white LED lamp. [k] 35 W green LED lamp (520 nm). [l] 110 °C, 60 mg catalyst for 1 mmol of substrate, no clear mechanism. [m] In the presence of TEMPO. [n] In the presence of benzoquinone.

tively. Therefore, the development of highly selective heterogeneous metal-free catalysts for selective synthesis of imine under mild conditions (at room temperature and solvent free) using simple air is highly desirable.

CTFs, owing their large surface area, different N-sites and surface basicity might be efficient solid base catalysts for highly selective formation of imine from the oxidative dimerization of amines. To explore this, the oxidative coupling of benzyl amine (**1a**) was chosen as a model reaction using pyz-CTF-5-500 CTF as catalyst under 1 atm of O₂ as green oxidant in different solvents at 40 °C for 12 h (Table S4, entry 1–4). To our delight, CH₃CN was found to be the best solvent, giving 60% of conversion of **1a** (from the ¹H NMR analysis). Surprisingly, allowing the same reaction for 24 h, 100% conversion of **1a** was observed with 86% yield of *N*-benzyl-1-phenylmethanimine (**2a**). In order to further explore the effect of other CTFs, reactions were continued in the same conditions using other CTFs as catalyst.

From the ¹H NMR results (Table 3), it was found that isox-CTF-5-400 showed the best yield for the formation of **2a**. Notably, the catalytic activity is comparable with the other isox-CTF and pyz-CTFs (entries 1, 2, and 4; Table 3), higher than acac-CTF (entry 5; Table 3) and slightly lower than CTF-1-400 (entry 6; Table 3). The observed catalytic properties are in accordance with the basicity of the respective CTFs (Table 2).

Furthermore, the same reactions were repeated under air (entry 7), neat (no solvent, entry 8) and even at room temperature (entry 9) using CTF-1-400. Surprisingly in each case, >99% of **2a** was obtained selectively. The reactions were also repeated using isox-CTF-5-400 and >90% selectivity for **2a** was observed. In comparison with the reported solid catalyst (entry 8–15; Table 3), CTFs showed the best catalytic activity for aerobic oxidative dimerization benzylamine under mild reaction conditions. Very recently Xu et al. used CTF-P (obtained by using 1,4-dicyanobenzene and ZnCl₂ in 1:1 ratio for 40 h) as metal-free catalyst for the oxidation of amine at elevated temperature (120 °C) using methanol as solvent (entry 15, Table 3).^[33g] However, the catalyst showed low reactivity at ambient temperature (< 100 °C). Surprisingly, in the present case using CTF-1 in CH₃CN, a high reactivity is observed even in ambient conditions (entry 6, Table 3). This might be due to the nature of solvent that enables high dispersion of substrate and catalyst in the reaction medium. In addition, the conditions used to synthesize CTF-1-400 and CTF-P result in CTF materials with differing surface areas, pore volumes, and surface basic properties and hence showed difference reactivity. Therefore, in the present case, the synthesis conditions of CTF and the characteristics of catalyst and solvent played important role to obtain high reactivity under ambient conditions.

To investigate the reaction performance with CTF-1-400 in detail, progress of the reaction was supervised using in situ ¹H NMR analysis with CD₃CN as solvent. As shown in Figure 7, **2a** was the sole product during the whole reaction. Surprisingly, the reaction started immediately, unlike MOF-253^[33d] (entry 14, Table 3) where an induction period was noticed. To gain more insight into the radical mechanism of the reaction, TEMPO (2,2,6,6-tetramethylpiperidin-1-yl)oxidanyl as free radical scavenger was added to the reaction. However, from the ¹H NMR analysis, it was found that TEMPO did not affect the formation of **2a** (entry 16, Table 3), and hence, a radical mechanism for the reaction can be ruled out.

Therefore, it can be proposed that different N-sites, surface basicity, and defects of CTF easily activate substrate **1a** and O₂ to initiate the reaction.^[33b] Furthermore, these N-sites can serve as reversible adsorption sites for the substrate **1a** and the product **2a** to obtain higher conversion and selectivity. A pro-

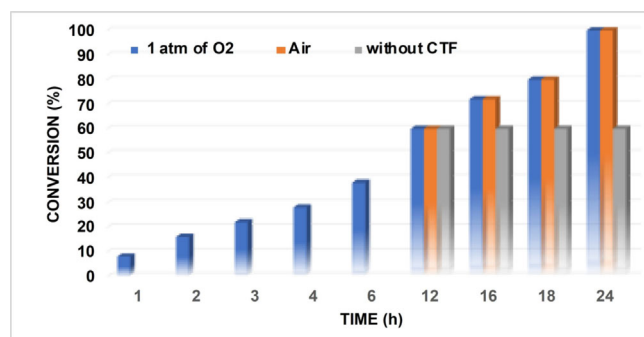
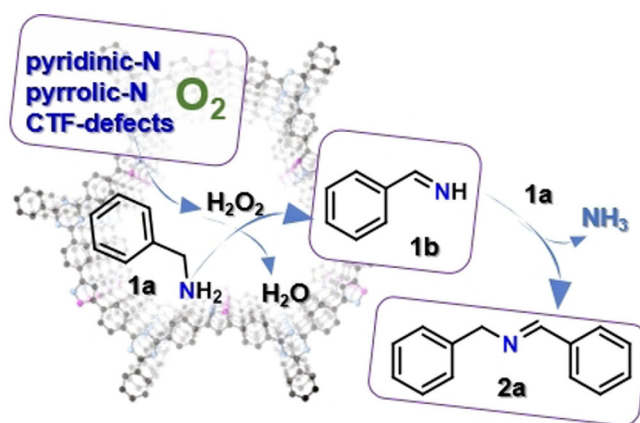


Figure 7. Conversion of **1a** using CTF-1-400 with reaction times using 1 atm of O₂. After 12 h the reaction was split into two: (i) pure O₂ removed and reaction continued (Air), and (ii) CTF-1-400 was filtered out after 12 h and reaction continued under pure (without CTF).



Scheme 2. Proposed reaction pathway for CTF catalyzed oxidative dimerization of **1a** to **2a**.

posed reaction mechanism is shown in Scheme 2. In the beginning of the reaction, substrate **1a** and O₂ were activated by CTF and subsequently transformed into benzylimine (**1b**) and H₂O₂ as intermediate, respectively. In situ ¹H NMR analysis was performed to detect the formation of H₂O₂. However, the absence of a peak at around 10.95 ppm^[33e] clearly indicates that H₂O₂ was immediately consumed by another **1a** to form **1b**. Further, upon use of benzoquinone as superoxide scavenger, the reaction stopped immediately and **2a** was not noticed from the NMR analysis (entry 17, Table 3). This observation clearly confirmed the formation of H₂O₂ in the reaction mixture. Finally, the intermediate **1b** owing to its highly unstable nature, immediately reacts with another molecule of **1a** to form product **2a**. Notably, during the reaction, the peak corresponding to the formation benzaldehyde^[32,33c-g] was not noticed from the NMR analysis. This ruled out the hydrolysis of **1b** to aldehyde and its reaction with **1a** to form **2a**. This observation strongly suggests benzylimine (**1b**) as a sole intermediate during this whole reaction.

To further explore the effect of heterogeneity and O₂, the reaction was stopped after 12 h of reaction time, cap of the vial was opened to remove all O₂ and further stirred for 12 h. Notably the reaction, did not stop even in the absence of O₂. This result again supported the fact that oxidation of amine to imine can be achieved simply under air (Figure 7; entry 7, Table 3). However, when the CTF is filtered out of the reaction after 12 h, the reaction stops immediately (Figure 7). This clearly indicates that CTF has a significant role in the oxidation reaction. Furthermore, the recyclability, reusability and reproducibility test—up to five cycles (Figure S17)—confirmed CTF as an extremely stable and solid porous base catalyst for aerobic oxidative dimerization of amine to imine under mild conditions. At the same time, larger surface area, N content, porosity, and surface basicity of CTFs play important roles in achieving high reactivity and selectivity.

Conclusions

In this study, a simple chemical transformation of one dinitrile linker (4,4'-malonyldibenzonitrile) (acac) to two other dinitrile

linkers (4,4'-(1*H*-pyrazole-3,5-diyl)dibenzonitrile (pyz) and 4,4'-(isoxazole-3,5-diyl)dibenzonitrile (isox)) was performed. Using them, two new sets of CTF materials (pyz-CTF and isox-CTF) with different functional groups were synthesized under ionothermal conditions, thoroughly characterized and explored for carbon capture storage and metal-free heterogeneous catalysis. Among all, isox-CTF-5-400 showed the best CO₂ capture (4.9 mmol g⁻¹ at 273 K and 1 bar) and CO₂/N₂ selectivity (28). Further, TPD-CO₂ analysis confirmed that the surface basicity of CTF is equally responsible as the surface area and the pore volume for enhanced CO₂ uptake. In addition, these new CTF materials showed excellent catalytic activity as an efficient solid porous base catalyst for aerobic oxidation of amine to imine in mild conditions using simple air as terminal oxidant. The mechanism of the reaction suggested that benzyl-imine was the sole intermediate during the reaction and was obtained by direct activation of benzylamine and O₂ through the basic nitrogen sites present in the CTF material. CTF with the highest basicity, showed best reactivity for the oxidation reaction.

Acknowledgements

H.S.J. thanks FWO [PEGASUS]² Marie Skłodowska-Curie Grant agreement No. 665501 for Incoming post-doctoral fellowship. C.K. and P.V.D.V. acknowledges the Research Board of Ghent University (GOA010-17, BOF GOA2017000303) for the PhD funding. K.V.H. thanks the Hercules Foundation (project AUGÉ/11/029 "3D-SPACE: 3D Structural Platform Aiming for Chemical Excellence") and the Special Research Fund (BOF)—UGent (project 01N03217) for funding. The authors would like to thank Dr. Jeroen De Decker for his help in IAST calculations and Funda Alic for CHNS analysis.

Conflict of interest

The authors declare no conflict of interest.

Keywords: building block transformation • carbon capture storage • covalent triazine frameworks • heterogeneous catalysis • porous materials

- [1] a) S. Kramer, N. R. Bennedsen, S. Kegnæs, *ACS Catal.* **2018**, *8*, 6961–6982; b) Y. Zhang, S. N. Riduan, *Chem. Soc. Rev.* **2012**, *41*, 2083–2094; c) P. Kaur, J. T. Hupp, S. T. Nguyen, *ACS Catal.* **2011**, *1*, 819–835.
- [2] a) A.-H. Lu, S. Dai, *Porous Materials for Carbon Dioxide Capture*, Springer, Berlin, **2014**; b) L. Zou, Y. Sun, S. Che, X. Yang, X. Wang, M. Bosch, Q. Wang, H. Li, M. Smith, S. Yuan, *Adv. Mater.* **2017**, *29*, 1700229; c) E. S. Sanz-Pérez, C. R. Murdock, S. A. Didas, C. W. Jones, *Chem. rev.* **2016**, *116*, 11840–11876; d) Y. S. Bae, R. Q. Snurr, *Angew. Chem. Int. Ed.* **2011**, *50*, 11586–11596; *Angew. Chem.* **2011**, *123*, 11790–11801; e) D. M. D'Alessandro, B. Smit, J. R. Long, *Angew. Chem. Int. Ed.* **2010**, *49*, 6058–6082; *Angew. Chem.* **2010**, *122*, 6194–6219.
- [3] a) R. Rinaldi, F. Schüth, *Energy & Environmental Sci.* **2009**, *2*, 610–626; *Environmental Sci.* **2009**, *2*, 610–626; b) R. Palkovits, M. Antonietti, P. Kuhn, A. Thomas, F. Schüth, *Angew. Chem. Int. Ed.* **2009**, *48*, 6909–6912; *Angew. Chem.* **2009**, *121*, 7042–7045; c) A. Thomas, *Angew. Chem. Int. Ed.* **2010**, *49*, 8328–8344; *Angew. Chem.* **2010**, *122*, 8506–8523.
- [4] a) Y. Zhang, S. Jin, *Polymer* **2018**, *11*, 31; b) J. Artz, *ChemCatChem* **2018**, *10*, 1753–1771; c) M. Liu, L. Guo, S. Jin, B. Tan, *J. Mater. Chem. A* **2019**, *7*, 5153–5172; d) P. Puthiaraj, Y.-R. Lee, S. Zhang, W.-S. Ahn, *J. Mater. Chem. A* **2016**, *4*, 16288–16311.
- [5] a) S. Hug, L. Stegbauer, H. Oh, M. Hirscher, B. V. Lotsch, *Chem. Mater.* **2015**, *27*, 8001–8010; b) P. Katekomol, J. R. M. Roeser, M. Bojdys, J. Weber, A. Thomas, *Chem. Mater.* **2013**, *25*, 1542–1548; c) P. Kuhn, M. Antonietti, A. Thomas, *Angew. Chem. Int. Ed.* **2008**, *47*, 3450–3453; *Angew. Chem.* **2008**, *120*, 3499–3502.
- [6] a) L. Tao, F. Niu, C. Wang, J. Liu, T. Wang, Q. Wang, *J. Mater. Chem. A* **2016**, *4*, 11812–11820; b) J. Du, Y. Liu, R. Krishna, Y. Yu, Y. Cui, S. Wang, Y. Liu, X. Song, Z. Liang, *ACS Appl. Mater. Interfaces* **2018**, *10*, 26678–26686.
- [7] S. Hug, M. B. Mesch, H. Oh, N. Popp, M. Hirscher, J. Senker, B. V. Lotsch, *J. Mater. Chem. A* **2014**, *2*, 5928–5936.
- [8] W. Yu, S. Gu, Y. Fu, S. Xiong, C. Pan, Y. Liu, G. Yu, *J. Catal.* **2018**, *362*, 1–9.
- [9] a) S. H. Je, H. J. Kim, J. Kim, J. W. Choi, A. Coskun, *Adv. Funct. Mater.* **2017**, *27*, 1703947; b) G. Wang, K. Leus, H. S. Jena, C. Krishnaraj, S. Zhao, H. Depauw, N. Tahir, Y.-Y. Liu, P. Van Der Voort, *J. Mater. Chem. A* **2018**, *6*, 6370–6375; c) F. Xu, S. Yang, G. Jiang, Q. Ye, B. Wei, H. Wang, *ACS Appl. Mater. Interfaces* **2017**, *9*, 37731–37738; d) Y. Zhao, K. X. Yao, B. Teng, T. Zhang, Y. Han, *Energy & Environmental Sci.* **2013**, *6*, 3684–3692; *Environmental Sci.* **2013**, *6*, 3684–3692.
- [10] a) S. Mukherjee, M. Das, A. Manna, R. Krishna, S. Das, *J. Mater. Chem. A* **2019**, *7*, 1055–1068; b) S. Mukherjee, M. Das, A. Manna, R. Krishna, S. Das, *Chem. Mater.* **2019**, *31*, 3929–3940.
- [11] a) O. Buyukcagir, S. H. Je, S. N. Talapaneni, D. Kim, A. Coskun, *ACS Appl. Mater. Interfaces* **2017**, *9*, 7209–7216; b) X. Zhu, C. Tian, G. M. Veith, C. W. Abney, J. R. M. Dehault, S. Dai, *J. Am. Chem. Soc.* **2016**, *138*, 11497–11500; c) K. Park, K. Lee, H. Kim, V. Ganesan, K. Cho, S. K. Jeong, S. Yoon, *J. Mater. Chem. A* **2017**, *5*, 8576–8582; d) K. Yuan, C. Liu, L. Zong, G. Yu, S. Cheng, J. Wang, Z. Weng, X. Jian, *ACS Appl. Mater. Interfaces* **2017**, *9*, 13201–13212; e) M. J. Bojdys, J. Jeromenok, A. Thomas, M. Antonietti, *Adv. Mater.* **2010**, *22*, 2202–2205; f) H. S. Jena, C. Krishnaraj, G. Wang, K. Leus, J. Schmidt, N. Chaoui, P. Van Der Voort, *Chem. Mater.* **2018**, *30*, 4102–4111; g) B. Dong, D.-Y. Wang, W.-J. Wang, *Microporous Mesoporous Mater.* **2020**, *292*, 109765.
- [12] a) A. Bavykina, H.-H. Mautscke, M. Makkee, F. Kapteijn, J. Gascon, F. X. Llabrés i Xamena, *CrystEngComm* **2017**, *19*, 4166–4170; b) C. E. Chan-Thaw, A. Villa, L. Prati, A. Thomas, *Chem. Eur. J.* **2011**, *17*, 1052–1057; c) T. He, L. Liu, G. Wu, P. Chen, *J. Mater. Chem. A* **2015**, *3*, 16235–16241; d) A. V. Bavykina, E. Rozhko, M. G. Goesten, T. Wezendonk, B. Seoane, F. Kapteijn, M. Makkee, J. Gascon, *ChemCatChem* **2016**, *8*, 2217–2221; e) A. V. Bavykina, A. I. Olivos-Suarez, D. Osadchii, R. Valecha, R. Franz, M. Makkee, F. Kapteijn, J. Gascon, *ACS Appl. Mater. Interfaces* **2017**, *9*, 26060–26065; f) G. H. Gunasekar, K. Park, V. Ganesan, K. Lee, N.-K. Kim, K.-D. Jung, S. Yoon, *Chem. Mater.* **2017**, *29*, 6740–6748; g) A. K. Beine, A. J. Krüger, J. Artz, C. Weidenthaler, C. Glotzbach, P. J. Hausoul, R. Palkovits, *Green Chem.* **2018**, *20*, 1316–1322; h) J. Artz, R. Palkovits, *ChemSusChem* **2015**, *8*, 3832–3838; i) Q.-Q. Dang, C.-Y. Liu, X.-M. Wang, X.-M. Zhang, *ACS Appl. Mater. Interfaces* **2018**, *10*, 27972–27978; j) C. E. Chan-Thaw, A. Villa, D. Wang, V. D. Santo, A. Orbelli Biroli, G. M. Veith, A. Thomas, L. Prati, *ChemCatChem* **2015**, *7*, 2149–2154; k) X. Lan, C. Du, L. Cao, T. She, Y. Li, G. Bai, *ACS Appl. Mater. Interfaces* **2018**, *10*, 38953–38962; l) N. Tahir, F. Muniz-Miranda, J. Everaert, P. Tack, T. Heugebaert, K. Leus, L. Vincze, C. V. Stevens, V. Van Speybroeck, P. Van Der Voort, *J. Catal.* **2019**, *371*, 135–143.
- [13] a) T. T. Liu, R. Xu, J. D. Yi, J. Liang, X. S. Wang, P. C. Shi, Y. B. Huang, R. Cao, *ChemCatChem* **2018**, *10*, 2036–2040; b) J. Roeser, K. Kailasam, A. Thomas, *ChemSusChem* **2012**, *5*, 1793–1799.
- [14] L. Zhao, S. Shi, M. Liu, G. Zhu, M. Wang, W. Du, J. Gao, J. Xu, *Green Chem.* **2018**, *20*, 1270–1279.
- [15] E. Troschke, K. D. Nguyen, S. Paasch, J. Schmidt, G. Nickler, I. Senkovska, E. Brunner, S. Kaske, *Chem. Eur. J.* **2018**, *24*, 18629–18633.
- [16] Y. J. Lee, S. N. Talapaneni, A. Coskun, *ACS Appl. Mater. Interfaces* **2017**, *9*, 30679–30685.
- [17] G. Zhu, S. Shi, M. Liu, L. Zhao, M. Wang, X. Zheng, J. Gao, J. Xu, *ACS Appl. Mater. Interfaces* **2018**, *10*, 12612–12617.

- [18] G. Tuci, A. Iemhoff, H. Ba, L. Luconi, A. Rossin, V. Papaefthimiou, R. Palkovits, J. Artz, C. Pham-Huu, G. Giambastiani, *Beilstein J. Nanotechnol.* **2019**, *10*, 1217–1227.
- [19] R. O. Diffraction in CrysAlisPro Software System, Vol. Rigaku Corporation Oxford, UK, **2018**.
- [20] O. V. Dolomanov, L. J. Bourhis, R. J. Gildea, J. A. Howard, H. Puschmann, *J. Appl. Crystallogr.* **2009**, *42*, 339–341.
- [21] G. M. Sheldrick, *Acta Crystallogr. Sect. A* **2008**, *64*, 112–122.
- [22] S. Ren, M. J. Bojdys, R. Dawson, A. Laybourn, Y. Z. Khimyak, D. J. Adams, A. I. Cooper, *Adv. Mater.* **2012**, *24*, 2357–2361.
- [23] K. Wang, L. M. Yang, X. Wang, L. Guo, G. Cheng, C. Zhang, S. Jin, B. Tan, A. Cooper, *Angew. Chem. Int. Ed.* **2017**, *56*, 14149–14153; *Angew. Chem.* **2017**, *129*, 14337–14341.
- [24] S. Y. Yu, J. Mahmood, H. J. Noh, J. M. Seo, S. M. Jung, S. H. Shin, Y. K. Im, I. Y. Jeon, J. B. Baek, *Angew. Chem. Int. Ed.* **2018**, *57*, 8438–8442; *Angew. Chem.* **2018**, *130*, 8574–8578.
- [25] G. Wang, K. Leus, S. Zhao, P. Van Der Voort, *ACS Appl. Mater. Interfaces* **2018**, *10*, 1244–1249.
- [26] C. Krishnaraj, H. S. Jena, K. Leus, H. Freeman, L. G. Benning, P. Van Der Voort, *J. Mater. Chem. A* **2019**, *7*, 13188–13196.
- [27] D. Y. Osadchii, A. I. Olivos-Suarez, A. V. Bavykina, J. Gascon, *Langmuir* **2017**, *33*, 14278–14285.
- [28] H. Naims, *Environ. Sci. Pollut. Res. Int.* **2016**, *23*, 22226–22241.
- [29] S. Keskin, T. M. van Heest, D. S. Sholl, *ChemSusChem* **2010**, *3*, 879–891.
- [30] G. Tuci, M. Pilaski, H. Ba, A. Rossin, L. Luconi, S. Caporali, C. Pham-Huu, R. Palkovits, G. Giambastiani, *Adv. Funct. Mater.* **2017**, *27*, 1605672.
- [31] S. K. Das, S. Mondal, S. Chatterjee, A. Bhaumik, *ChemCatChem* **2018**, *10*, 2488–2495.
- [32] F. Su, S. C. Mathew, L. Möhlmann, M. Antonietti, X. Wang, S. Blechert, *Angew. Chem. Int. Ed.* **2011**, *50*, 657–660; *Angew. Chem.* **2011**, *123*, 683–686.
- [33] a) H. Huang, J. Huang, Y.-M. Liu, H.-Y. He, Y. Cao, K.-N. Fan, *Green Chem.* **2012**, *14*, 930–934; b) B. Chen, L. Wang, W. Dai, S. Shang, Y. Lv, S. Gao, *ACS Catal.* **2015**, *5*, 2788–2794; c) P. Yang, J. Zhang, D. Liu, M. Liu, H. Zhang, P. Zhao, C. Zhang, *Microporous Mesoporous Mater.* **2018**, *266*, 198–203; d) X. Qiu, C. Len, R. Luque, Y. Li, *ChemSusChem* **2014**, *7*, 1684–1688; e) F. Raza, J. H. Park, H.-R. Lee, H.-I. Kim, S.-J. Jeon, J.-H. Kim, *ACS Catal.* **2016**, *6*, 2754–2759; f) Y. Zhi, K. Li, H. Xia, M. Xue, Y. Mu, X. Liu, *J. Mater. Chem. A* **2017**, *5*, 8697–8704; g) H. Zheng, S. Shi, X. Wang, L. Zhao, G. Zhu, M. Liu, J. Gao, J. Xu, *ChemistrySelect* **2019**, *4*, 5073–5080.

Manuscript received: August 27, 2019

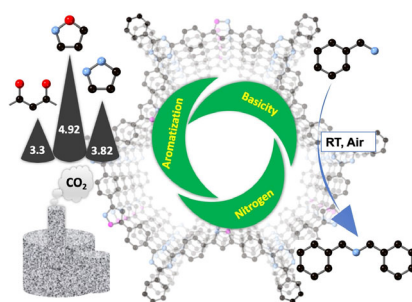
Revised manuscript received: October 4, 2019

Accepted manuscript online: October 11, 2019

Version of record online: ■■■■■, 0000

FULL PAPER

The effect of building block transformations and ligand aromatization to tune the surface area, N content, pore characteristics, and surface basicity of covalent triazine-based frameworks is reported in this work, to achieve enhanced CO₂ uptake and metal-free catalytic activity.



Carbon Storage

H. S. Jena,* C. Krishnaraj, J. Schmidt,
K. Leus, K. Van Hecke, P. Van Der Voort*



Effect of Building Block
Transformation in Covalent Triazine-
Based Frameworks for Enhanced CO₂
Uptake and Metal-Free Heterogeneous
Catalysis

